



Article

# Different Conditions of Formation Experienced by Iron Meteorites as Suggested by Neutron Diffraction Investigation

Francesco Grazzi <sup>1</sup>, Antonella Scherillo <sup>2</sup>, Vanni Moggi-Cecchi <sup>3</sup>, Marco Morelli <sup>4</sup>, Giovanni Pratesi <sup>5</sup>  and Stefano Caporali <sup>1,6,\*</sup> 

<sup>1</sup> Consiglio Nazionale delle Ricerche, Istituto dei Sistemi Complessi, Via Madonna del Piano 10, 50019 Sesto Fiorentino, Italy; francesco.grazzi@fi.isc.cnr.it

<sup>2</sup> ISIS Facility Rutherford Appleton Laboratory, Didcot OX11, UK; antonella.scherillo@stfc.ac.uk

<sup>3</sup> Museo di Storia Naturale, Università degli Studi di Firenze, Via La Pira 4, 50121 Firenze, Italy; vanni.moggicecchi@unifi.it

<sup>4</sup> Museo di Scienze Planetarie-Fondazione Parsec, Via Galcianese 20H, 59100 Prato, Italy; marcomorelli7388@gmail.com

<sup>5</sup> Dipartimento di Scienze della Terra, Università degli Studi di Firenze, Via La Pira 4, 50121 Firenze, Italy; giovanni.pratesi@unifi.it

<sup>6</sup> Dipartimento Ingegneria Industriale, Via S. Marta 3, 50139 Firenze, Italy

\* Correspondence: stefano.caporali@unifi.it; Tel.: +39-055-457-3119

Received: 22 September 2017; Accepted: 8 January 2018; Published: 12 January 2018

**Abstract:** In this communication, we report the results of a preliminary neutron diffraction investigation of iron meteorites. These planetary materials are mainly constituted by metallic iron with variable nickel contents, and, owing to their peculiar genesis, are considered to offer the best constrains on the early stages of planetary accretion. Nine different iron meteorites, representative of different chemical and structural groups, thought to have been formed in very different pressure and temperature conditions, were investigated, evidencing variances in crystallites size, texturing, and residual strain. The variability of these parameters and their relationship, were discussed in respect to possible diverse range of petrological conditions, mainly pressure and cooling rate, experienced by these materials during the crystallization stage and/or as consequence of post accretion events.

**Keywords:** neutron scattering; iron meteorites; residual strain; texturing

## 1. Introduction

It is currently accepted that, in the Solar System, planets formed by collisional growth from smaller bodies, which size ranges from powder to protoplanets [1]. There is a growing consensus that these bodies accreted early in the Solar System's history since <sup>26</sup>Al, which has a half-life of only 0.7 Myr, is considered the main source of the heat that melt the asteroids, allowing for the heavier components to separate from silicates forming the metallic cores [2]. After a more or less rapid crystallization, these protoplanets were shattered, and sometimes scattered, by asteroidal hypervelocity impacts. Shortly after the impacts, a large part of the mass aggregated again under gravity effect; nevertheless, when the velocity of the ejected fragments overcame the escape velocity, they abandoned the asteroid and travelled in the space taking on their own orbit. Then, eventually, were captured by Earth's gravity crossing its atmosphere as meteors, and, some of them, falling on its surface as meteorites.

Iron meteorites are assumed to be fragments of asteroids cores produced by these primordial large impacts. If meteorites are large enough (more than a cubic decimeter), reheating effects yielded when they enter the Earth's atmosphere only affect their very external portions, leaving the interior

unaffected. This offers the possibility to study the pristine materials crystallized during the very early stages of planetary accretions, from which glimpses of the geophysical constrain of the processes that took place a few billions of years ago can be speculated.

The overwhelming bulk mineralogy of iron meteorites consists of Fe-Ni alloys; i.e., iron ( $\alpha$ -(Fe, Ni), BCC structure, historically known as *kamacite*) and taenite ( $\gamma$ -(Fe, Ni), FCC structure). It is generally accepted that the *kamacite* phase, occurring as elongated plates or lamellae, is generated by a solid-state phase transformation at the taenite/taenite grain boundary when the material is slowly cooled down [2]. As a consequence, the fine intergrowth of these two phases, named Widmanstätten patterns, constitutes a peculiar feature of the most part of iron meteorites. The thickness of the *kamacite* lamellae (*kamacite* bandwidth) is primarily dictated by the bulk chemical composition, i.e., initial nickel content, the size of the pristine taenite crystals and the cooling rate; the higher the nickel content and the faster the cooling rate, the smaller the *kamacite* bandwidths [3].

The detailed knowledge of the texture of a meteorite, i.e., the size, shape, and distribution of crystallographic orientations of residual taenite crystal and *kamacite* lamellae, can provide useful insight about the process by which the materials formed and the composition of the parent asteroid. Traditionally, this goal is achieved by means of metallographic observation on specifically cut and polished portions of the sample. This approach is intrinsically destructive and cannot provide information about the residual stresses of the material. In recent years, techniques based upon penetrative probes such as hard X-rays radiations or neutrons gained a prominent position in the study of the metallic material crystal structure [4–6]. Respect to the classical approach these techniques offer the main advantage of being non-destructive. For such reason, they can be applied to determine texture and crystallographic features of precious or scarcely available samples, such as meteorites. For example, Hofler and coworkers [7] studied the texture of the Gibeon meteorite by means of neutron diffraction, Peetermans and coworkers [8] used energy-selective neutron imaging to obtain the texture of the Mont Dieu meteorite while neutron tomography was used to achieve three-dimensional (3D) spatial reconstruction of crystals in some iron meteorites [9]. Alternatively, conventional X-ray transmission radiography was applied to study the orientation of *kamacite* lamellae [10], and both, hard X-ray photoemission electron microscopy (HX-PEEM) [11], and X-ray synchrotron diffraction [12] were used to determine the metallographic properties of the Gibeon meteorite. However, to the best of our knowledge, these studies were limited to a very little number of meteorite samples and no determination of residual strain was attempted. Indeed, the presence of residual crystal lattice strain can be related to peculiar petrological conditions experienced by the samples during or after their formation. In accordance with the principal geophysics' textbooks we assumed that crystallization from metallic melt took place in hydrostatic conditions. If so, homogeneous residual (compressive) strain can be attributed to the pressure experienced during the crystallization stage, strictly related to the size of the parent asteroid. Again, inhomogeneous or directional strains can be related to intense directional stresses experienced by the meteorite after its crystallization, namely hypervelocity asteroidal impacts whose effects were not cancelled by thermal annealing.

In this paper, we present the results of a preliminary investigation aiming to assess the feasibility of the analytical approach to cope with extraterrestrial metallic materials. On a set of nine iron or stony-iron meteorites belonging to different chemical groups, metallographic and structural parameters were determined via neutron diffraction investigation. Among this set of samples, large differences in texturing and crystallographic domains size were determined. Texturing means discrepancy between the diffraction pattern generated by a microstructurally oriented sample with respect to the one generated by an ideal isotropic homogeneous sample (namely a randomly oriented powder in the crystallographic meaning). By comparison with the chemical data and metallographic observations available in literature the new data here presented were tentatively attributed to possible different petrologic conditions experienced by these materials during, or after, the crystallization stage.

## 2. Materials and Methods

The meteorite samples were obtained from the Museo di Scienze Planetarie-Fondazione Parsec (Prato, Italy) and the Museo di Storia Naturale dell'Università degli Studi di Firenze (Firenze, Italy). Table 1 summarizes the characteristics of the investigated samples.

**Table 1.** Summary of the investigated samples. In the shape and size column, the term *whole* refers to an uncut sample (including the annealed external portion) while *cut* refers to internal portions extracted from the unaltered core of larger samples.

| Catalog Number | Sample Name          | Shape and Size (L × W × H) (cm <sup>3</sup> ) | Chemical Classif. | Structural Classif.          | Cooling Rate (°K·Ma <sup>-1</sup> ) [13] | Proposed Parent Asteroid's Size [13]     |
|----------------|----------------------|---|-------------------|------------------------------|--|--|
| MSP-PL2391     | Castiglione del Lago | <i>Whole</i><br>5 × 5 × 4                     | IAB-MG            | Coarsest octahedrite (Ogg)   | 1–5                                      | >150                                     |
| MSN-RI3221     | Campo del cielo      | <i>Cut</i><br>2 × 2 × 1                       | IAB-MG            | Hexahedrite (H)              |  |  |
| MSP-PL5067     | Sikhote Alin         | <i>Whole</i><br>2 × 2 × 3                     | IIAB              | Coarsest octahedrite (Ogg)   | 6–12                                     | 90–130 km                                |
| MSN-RI3219     | Sikhote Alin         | <i>Cut</i><br>20 × 10 × 4                     | IIAB              | Coarsest octahedrite (Ogg)   |  |  |
| MSN-RI3220     | Agoudal              | <i>Cut</i><br>4 × 4 × 3                       | IIAB              | Coarse octahedrite (Og)      |  |  |
| MSN-RI3222     | Muonionalusta        | <i>Cut</i><br>4 × 1 × 1                       | IV A              | Fine octahedrite (Of)        | 100–6600                                 | ~300 km (lack of insulating mantle) [14] |
| MSN-RI3218     | Seymchan             | <i>Cut</i><br>3 × 3 × 4                       | Pallasite         | Coarse octahedrite (Og)      | 6–12                                     | 90–130 km                                |
| MSP-PL1412     | Mont Dieu            | <i>Cut</i><br>10 × 8 × 2                      | ungrouped         | Plessitic octahedrites (Off) | 100–150                                  | <50 [15]                                 |
| MSN-RI3282     | Gebel Kamil          | <i>Whole</i><br>3 × 2 × 2                     | ungrouped         | Ataxite (D)                  | 1400–17,000                              | small                                    |
| MSP-PL5069     | Chinga               | <i>Cut</i><br>7 × 6 × 1                       | ungrouped         | Ataxite (D)                  | 1400–17,000                              | small                                    |

The samples were analysed using the Time of Flight Diffractometer INES (Italian Neutron Experimental Station) [16,17] at the ISIS neutron spallation source [18] (Rutherford Appleton Laboratory, Didcot, UK). The average thermal neutron flux of INES is about of  $10^6$  n·cm<sup>-2</sup>·s<sup>-1</sup> [16] as measured through the integrated synchrotron proton current. After irradiation, the activation of the sample was measured using the Geiger counter provided on the beamline, and the samples were showing no activation at 5 min after removal from the beam-line.

The data reduction and focusing was performed using the Mantid code [19] and the data analysis on *kamacite* phase was carried on through the GSAS program [20] exploiting the EXPGUI interface [21]. The function peak profile used was number four since it is the one offering the best degree of detail in the diffraction peak shape analysis.

The microstructural properties were determined by analysing the shape and the relative intensity distribution of the *kamacite* diffraction peaks, while its lattice parameter ( $\alpha$ -(Fe, Ni), size of the BCC cell), directly related to the Fe-Ni relative concentration [22], were determined by peaks displacement and exploited to evaluate the nickel content. In the set of samples analysed, *kamacite* resulted the main phase, therefore we carried out the microstructural analysis of this phase alone in order to determine the properties of the material and the relationship with the crystallization and post-annealing conditions. The size of the crystallographic domains was determined by applying the Scherrer law [20,21], using the Lorentzian broadening of the peaks [20]. The degree of intensity of the third type microstrain [20,21] was semi-quantitatively determined by exploiting the Gaussian broadening parameter S400 [20,21]. Finally, since in the time of flight approach, every detector at fixed position, provides a complete diffraction pattern [16], therefore the texturing, i.e., the presence of preferred crystallographic orientation, was qualitatively evaluated by visualizing the diffraction patterns as a function of the scattering angle.

### 3. Results

A typical neutron diffraction pattern (Mont Dieu meteorite) is displayed in Figure 1. The scatter plot (crosses) depicts the experimental data while the line fitting obtained applying Rietveld refinement is represented by a red line. The two main phases, taenite and *kamacite*, were identified and the peaks were consistently labeled. The mismatch between fitting and experimental data depicted by the blue line represents the evidence of texturing (in the sample reported in Figure 1 show only modest discrepancy therefore, little or none texturing).

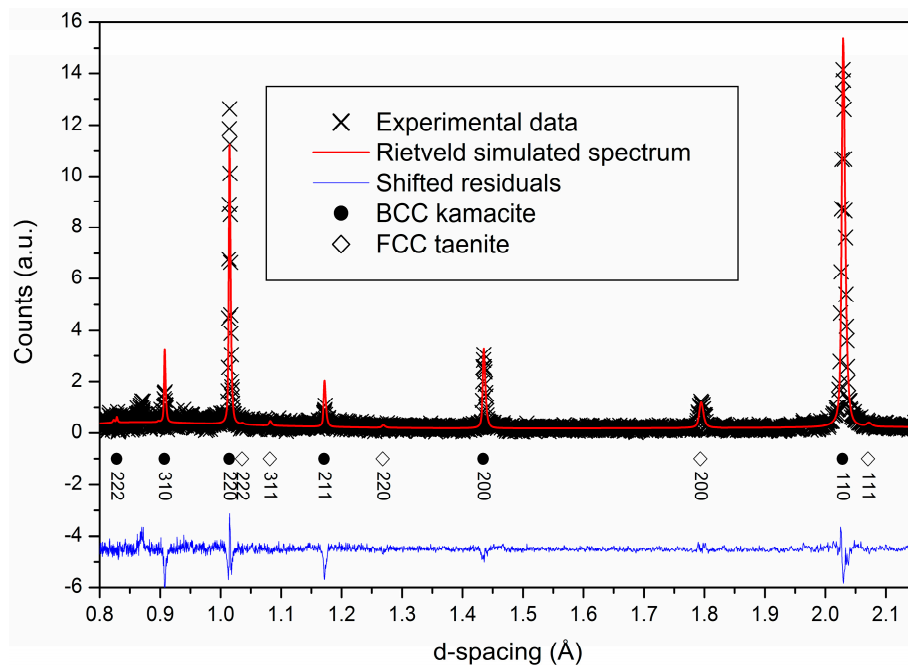


**Figure 1.** Rietveld analysis of the Mont Dieu sample diffraction pattern recorded by the  $^3\text{He}$  detector placed at  $2\theta = 90.565^\circ$ . In the picture are shown the experimental data points (crosses), the Rietveld refinement fit (continuous line), the reconstructed positions of the Bragg reflections (dots and diamonds) and the residuals of the fit (blue continuous line). The peak at  $0.87 \text{ \AA}$  is relative to the aluminum tape used to fix the samples.

Among the investigated samples, several cases returned a barely detectable taenite diffraction pattern. That is due to lower total amount of this phase with respect to *kamacite* and to the fact that taenite is usually distributed as intergranular precipitates around *kamacite* large grains. In such conditions, the level of disorder in the taenite crystallites is higher, resulting in weaker and broader diffraction peaks than the ones of *kamacite* [23]. Therefore, compositional and microstructural analyses were performed taking into account the *kamacite* data alone.

A qualitative evaluation of the texturing of each sample was obtained by observing the diffraction intensity distribution as a function of the scattering angle (refer to [16] for set-up and instrumental details). The diffraction patterns displayed in Figure 2 present two different trends: (a) the relative intensity of the peaks remains almost constant varying the scattering angle or (b) it changes significantly. In case (a), the crystalline structure of the samples is reasonably represented by randomly oriented crystallites. Chinga, Mont Dieu, and Gebel Kamil meteorites fall into this group. The (b) case, that shows a steep variation in the peak intensity as a function of the scattering angle, represents materials in which the crystals result preferentially oriented along few crystallographic directions (i.e., texturing). Seymchan, Muonionalusta, Campo del Cielo, Agoudal, and Castiglione del Lago meteorites fall into this group.

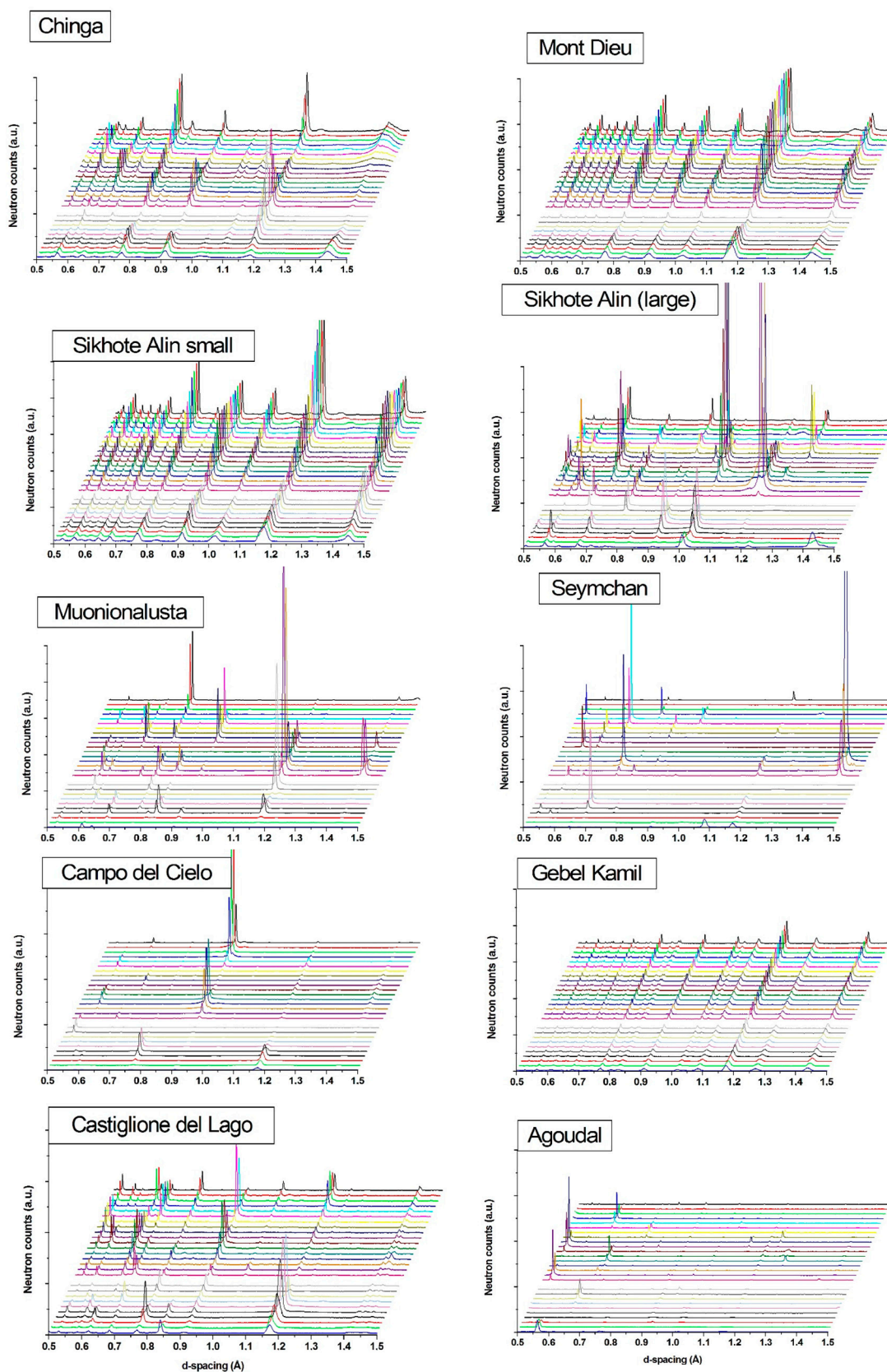


**Figure 2.** Diffraction patterns taken at different angles for the investigated samples. The name of the meteorite is labeled on the top left corner on every diffraction diagrams.

It is worth mentioning that two different samples of the same meteorite (Sikhote Alin) provided apparently contradictory results. The first one, which was cut from the bulk of a large specimen, exhibits a steep variation of the diffraction peaks intensity as function of the scattering angle (strong texturing), while the other, constituted by a whole little splint detached from the main mass during the atmosphere transit, does not show any variation in the diffraction peak relative intensity (no texturing). This opposite behavior displayed by a nominally same meteorite, is probably related to the aerodynamic heating that was experienced by the small sample. It is well known that reheating at sufficiently high temperature determines the  $\alpha$  to  $\gamma$  solid phase transition. After the fall, the rapid cooling stimulates *kamacite* recrystallization in a powder-like distribution. The same powder-like behavior is observed for the Gebel Kamil sample (Figure 2), which is a small whole fragment and reasonably was subjected to similar annealing experience. It is therefore reasonable to suppose that reheating due to the atmosphere transit heavily affects small (1–2 cm size) splints making their microstructure no more representative of the condition of the pristine meteorite. Vice versa, portions of larger fragments, like the one analyzed and displayed in Figure 2, result unaffected by the atmospheric reheating. A deeper investigation of this aspect will be demanded to future measurements on a properly prepared set of samples.

Table 2 displays the *kamacite* lattice parameters, namely the size of the cubic cell, as determined by the displacement of the diffraction peaks respect to the pure iron. By assuming that the observed lattice displacement can be attributed to the Ni content, the amount of Ni substituting Fe in *kamacite* lattice can be precisely evaluated [22]. The resulting Ni content in *kamacite* can be compared with the amount determined, in this phase, by chemical analysis (Table 2).

**Table 2.** Average nickel content (wt %) in the *kamacite* phase as determined by chemical analysis (measured Ni content, literature data) and calculated by the measured lattice parameter displacement with respect to pure iron (equivalent Ni content).

| Sample Name          | Kamacite Lattice Parameter (Å) | Equivalent Ni Content (wt %) | Measured Ni Content (wt %) | $\Delta$ |
|----------------------|--------------------------------|------------------------------|----------------------------|----------|
| Castiglione del Lago | 2.87008(4)                     | 8.6 ± 0.1                    | 6.5 ± 0.2 [24]             | +2.1     |
| Campo del cielo      | 2.86978(9)                     | 7.5 ± 0.3                    | 6.4 ± 0.1 [25]             | +1.1     |
| Sikhote Alin         | 2.86853(6)                     | 3.6 ± 0.1                    | 5.9 ± 0.1 [25]             | −2.3     |
| Agoudal              | 2.86945(8)                     | 6.3 ± 0.2                    | 5.5 ± 0.1 [26]             | +0.8     |
| Muonionalusta        | 2.86987(4)                     | 7.8 ± 0.1                    | 7.40 ± 0.03 [27]           | +0.4     |
| Seymchan             | 2.86934(4)                     | 5.9 ± 0.2                    | 5.3 ± 0.09 [28]            | +0.6     |
| Mont Dieu            | 2.86899(2)                     | 4.9 ± 0.1                    | 5.5 [15]                   | −0.6     |
| Gebel Kamil          | 2.86960(2)                     | 6.85 ± 0.08                  | -                          | nd       |
| Chinga               | 2.86921(3)                     | 5.5 ± 0.1                    | -                          | nd       |

In several cases, remarkable discrepancies were observed. A lower Ni content (larger elemental cell) was observed for the Sikhote Alin meteorite. This can be physically attributed to two reasons: (a) the presence of cell-enlarging elements (such as Co) and (b) to shear deformations [25]. However, chemical analysis ruled out the massive presence of cell-enlarging elements, therefore the observed difference can be reasonably attributed to shear deformation alone. Vice-versa, Ni contents significantly higher than the amount deduced from lattice parameter (smaller elemental cell) cannot be explained by the presence of massive amounts of foreign elements. Therefore, the most likely explanation of the observed lattice shrinkage can be tentatively attributed to different physical conditions that were experienced by the samples during the crystallization stage. Large parental asteroids, such as the one on which Castiglione del Lago and Campo del Cielo are supposed to be formed (see Table 1), would generate higher pressure contributing to compressive strains that cannot be removed if significant reheating would not have happened. On the other hand, meteorites formed within smaller bodies would have experienced much lower pressures, resulting in nearly unstressed lattices (Mont Dieu).

Finally, the third type strain values, obtained by fitting the Gaussian broadening of diffraction peaks of *kamacite* (using the S400 gaussian parameter of type 4 peak profile function [19]), were plotted as function of the crystallite size determined through the broadening of the Lorentzian peak profile, according to the Scherrer law (Figure 3). It is worth noting that the investigated samples can be tentatively grouped into three different sets: (1) samples characterized by small size crystallites and none or negligible internal stress (Figure 3, red circle); all of the coarse and coarsest octahedrites and the hexahedrite investigated in this work, fall within this group; (2) Samples characterized by small crystallites but high residual stress (Figure 3, blue circle); the finest grained meteorites (ataxite and plessitic octahedrite) fall in this group; and, (3) Samples characterized by larger crystallites and little or none internal stress (Figure 3, green circle) displayed by fine grained meteorites, such as Gebel Kamil and Muonionalusta.

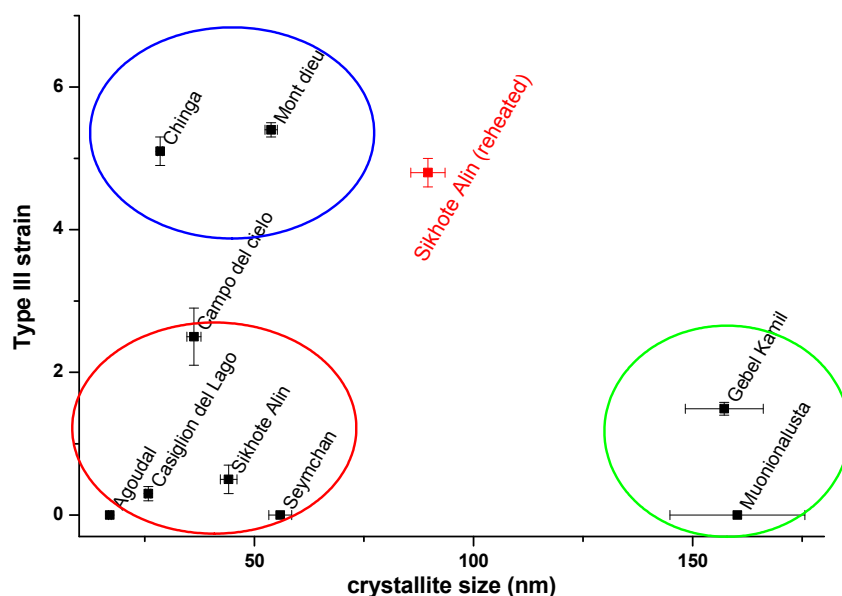


**Figure 3.** Third type strain versus crystallite size plot for the analyzed meteorite samples. Three different zones of the graph can be defined: small size-low strain (red circle), small size-high strain (blue circle) and larger size-low strain (green circle).

It is worth to highlight that the crystallite size is not strictly related to microstructure since both coarse and fine-grained iron meteorites present crystals of variable sizes. This is likely related to the post crystallization conditions experienced by the sample; reheating and long annealing would result in larger crystallites, whereas rapid cooling without post accretional annealing would result in smaller crystallites. Vice versa, residual internal strain is reasonably related to episodes of intense stress conditions without an adequate annealing experienced by the meteorites after crystallization. Asteroidal hypervelocity impacts with fragmentation of the solidified material, followed by an insufficient annealing time would account for these conditions [29]. Accordingly, meteorites characterized by evident plastic deformation, such as Chinga [30] and Mont Dieu [31], present the highest value of internal strain.

Noteworthy, the case of the little fragment of Sikhote Alin meteorite, witnesses the effect of atmospheric heating. Respect the pristine material, small samples experienced higher temperature during the atmospheric transit and successive rapid cooling. The heating was not high enough to affect their microstructure, but the effects of this rapid annealing are clearly detectable by the larger crystallites size and the higher internal strain.

#### 4. Conclusions

Nine different iron meteorites, representative of different chemical groups, were analysed by means of neutron scattering. The diffraction data evidenced remarkable differences among the investigated samples regarding texturing, crystallite sizes, and internal strain. Texturing differences can be related to variable crystallization conditions. Rapid cooling rate during the accretion stage or reheating followed by a rapid cooling could account for a highly textured material. Crystallite sizes and internal strain seem to be reasonably related to rapid post accretion annealing or plastic deformation, such as hypervelocity impacts, or, for tiny samples, the simple atmospheric transit. Finally, size discrepancies between the measured *kamacite* cell parameters and their theoretical value, determined accounting the relative Ni content, were observed and tentatively related to the different pressures that were experienced by the meteorite during the accretion stage.

For the first time, differences in the texturing, residual strain, and cell size in iron meteorites were recognized in a non-destructive way. Even if a systematic study involving a much larger number of meteorite samples would be recommended to confirm these preliminary data, the analytical approach here described may represent a new and powerful tool for the investigation of the petrochemical conditions ruling the very early stages of formation of the Solar System.

**Acknowledgments:** The cooperation Agreement No. 06/20018 between CNR and STFC, concerning collaboration in scientific research at the spallation neutron source ISIS (UK), is gratefully acknowledged. S.C. would like to thank Regione Toscana for financial support of the project LTSP through the fund POR FSE 2007–2013 (Obiettivo 2, Asse IV).

**Author Contributions:** F.G. and S.C. conceived and designed the experiments and together with A.S. performed the experiments and analyzed the data; G.P. and V.M.-C. analyzed the data; G.P. and M.M. provided the samples in study and discussed the data. All the authors contribute to the writing of the paper.

**Conflicts of Interest:** The authors declare no conflict of interest.

#### Abbreviations

|     |                     |
|-----|---------------------|
| BCC | body centered cubic |
| FCC | face centered cubic |

#### References

1. Kokubo, E.; Ida, S. Formation of Protoplanets from Planetesimals in the Solar Nebula. *Icarus* **2000**, *143*, 15–27. [[CrossRef](#)]
2. Goldstein, J.I.; Scott, E.R.D.; Chabot, N.L. Iron meteorites: Crystallization, thermal history, parent bodies, and origin. *Chem. Erde-Geochem.* **2009**, *69*, 293–325. [[CrossRef](#)]
3. Hopfe, W.D.; Goldstein, J.I. The metallographic cooling rate method revised: Application to iron meteorites and mesosiderites. *Meteorit. Planet. Sci.* **2001**, *36*, 135–154. [[CrossRef](#)]
4. Arletti, R.; Cartechini, L.; Rinaldi, R.; Giovannini, S.; Kockelmann, W.; Cardarelli, A. Texture analysis of bronze age axes by neutron diffraction. *Appl. Phys. A Mater. Sci. Process.* **2008**, *90*, 9–14. [[CrossRef](#)]
5. Siano, S.; Kockelmann, W.; Bafile, U.; Celli, M.; Iozzo, M.; Miccio, M.; Moze, O.; Pini, R.; Salimbeni, R.; Zoppi, M. Quantitative multiphase analysis of archaeological bronzes by neutron diffraction. *Appl. Phys. A Mater. Sci. Process.* **2002**, *74*, 1139–1142. [[CrossRef](#)]
6. Festa, G.; Caroppi, P.A.; Filabozzi, A.; Andreani, C.; Arancio, M.L.; Triolo, R.; Lo Celso, F.; Benfante, V.; Imberti, S. Composition and corrosion phases of Etruscan Bronzes from Villanovan Age. *Meas. Sci. Technol.* **2008**, *19*, 34004. [[CrossRef](#)]
7. Höfler, S.; Will, G.; Hamm, H.-M. Neutron diffraction pole figure measurements on iron meteorites. *Earth Planet. Sci. Lett.* **1988**, *90*, 1–10. [[CrossRef](#)]
8. Peetermans, S.; Grazzi, F.; Salvemini, F.; Lehmann, E.H.H.; Caporali, S.; Pratesi, G. Energy-selective neutron imaging for morphological and phase analysis of iron-nickel meteorites. *Analyst* **2013**, *138*, 5303–5308. [[CrossRef](#)] [[PubMed](#)]



9. Caporali, S.; Grazzi, F.; Salvemini, F.; Garbe, U.; Peetermans, S.; Pratesi, G. Structural characterization of iron meteorites through neutron tomography. *Minerals* **2016**, *6*, 14. [[CrossRef](#)]
10. Weiss, W.; Bunge, H.J. Diffraction contrast in X-ray radiographic images of octahedrite meteorites. *J. Appl. Crystallogr.* **2001**, *34*, 566–572. [[CrossRef](#)]
11. Kotsugi, M.; Wakita, T.; Taniuchi, T.; Maruyama, H.; Mitsumata, C.; Ono, K.; Suzuki, M.; Kawamura, N.; Ishimatsu, N.; Oshima, M.; et al. Direct metallographic analysis of an iron meteorite using hard X-ray photoelectron emission microscopy. *IBM J. Res. Dev.* **2011**, *55*, 13:1–13:5. [[CrossRef](#)]
12. Bunge, H.J.; Weiss, W.; Klein, H.; Wcislak, L.; Garbe, U.; Schneider, J.R. Orientation relationship of widmannstätten plates in an iron meteorite measured with high-energy synchrotron radiation. *J. Appl. Crystallogr.* **2003**, *36*, 137–140. [[CrossRef](#)]
13. Grady, M.; Pratesi, G.; Moggi Cecchi, V. *Atlas of Meteorites*; Cambridge University Press: Cambridge, UK, 2014.
14. Yang, J.; Goldstein, J.I.; Scott, E.R.D. Iron meteorite evidence for early formation and catastrophic disruption of protoplanets. *Nature* **2007**, *446*, 888–891. [[CrossRef](#)] [[PubMed](#)]
15. Desrousseaux, A.; Doukhan, J.C.; Leroux, H.; Van Duysen, J.C. An analytical electron microscope investigation of some pallasites. *Phys. Earth Planet. Inter.* **1997**, *103*, 101–115. [[CrossRef](#)]
16. Grazzi, F.; Celli, M.; Siano, S.; Zoppi, M. Preliminary results of the Italian neutron experimental station INES at ISIS: Archaeometric applications. *Nuovo Cim. Della Soc. Ital. Fis. C* **2007**, *30*, 59–65. [[CrossRef](#)]
17. Imberti, S.; Kockelmann, W.; Celli, M.; Grazzi, F.; Zoppi, M.; Botti, A.; Sodo, A.; Leo Imperiale, M.; de Vries-Melein, M.; Visser, D.; et al. Neutron diffractometer INES for quantitative phase analysis of archaeological objects. *Meas. Sci. Technol.* **2008**, *19*, 34003. [[CrossRef](#)]
18. ISIS. Available online: [www.isis.stfc.ac.uk](http://www.isis.stfc.ac.uk) (accessed on 1 January 2017).
19. Mantid. Available online: <http://www.mantidproject.org/> (accessed on 10 August 2017).
20. Larson, A.C.; Von Dreele, R.B. General Structure Analysis System (GSAS). *Los Alamos Natl. Lab. Rep.* **2000**, 86–748.
21. Toby, B.H. EXPGUI, a graphical user interface for GSAS. *J. Appl. Crystallogr.* **2001**, *34*, 210–213. [[CrossRef](#)]
22. Pearson, W.B. *A Handbook of Lattice Spacings and Structures of Metals and Alloys: International Series of Monographs on Metal Physics and Physical Metallurgy*; Pergamon Press Ltd.: Oxford, UK, 1964.
23. Grazzi, F.; Bartoli, L.; Siano, S.; Zoppi, M. Characterization of copper alloys of archaeometallurgical interest using neutron diffraction: A systematic calibration study. *Anal. Bioanal. Chem.* **2010**, *397*, 2501–2511. [[CrossRef](#)] [[PubMed](#)]
24. Moggi-Cecchi, V.; Herd, C.D.K.; Pratesi, G.; Caporali, S.; Chen, Y. Castelvechio and Castiglione del Lago: Two new Italian iron meteorites. *Eur. Phys. J. Plus* **2017**, *132*, 359. [[CrossRef](#)]
25. Rasmussen, K.L.; Greenway, T.J.L.; Gwozdz, R. The composition of kamacite in iron meteorites investigated by accelerator mass spectroscopy, neutron activation analysis and analytical electron microscopy. *Nucl. Instrum. Methods Phys. Res. Sect. B Beam Interact. Mater. Atoms* **1989**, *36*, 43–52. [[CrossRef](#)]
26. Ruzicka, A.; Grossman, J.; Bouvier, A.; Agee, C.B. The Meteoritical Bulletin, No. 103. *Meteorit. Planet. Sci.* **2017**, *52*, 1014. [[CrossRef](#)]
27. Reed, S.J.B. Electron-probe microanalysis of the metallic phases in iron meteorites. *Geochim. Cosmochim. Acta* **1965**, *29*, 535–549. [[CrossRef](#)]
28. Goldstein, J.I.; Yang, J.; Scott, E.R.D. Determining cooling rates of iron and stony-iron meteorites from measurements of Ni and Co at kamacite–taenite interfaces. *Geochim. Cosmochim. Acta* **2014**, *140*, 297–320. [[CrossRef](#)]
29. Kenkmann, T.; Trullenque, G.; Deutsch, A.; Hecht, L.; Ebert, M.; Salge, T.; Schäfer, F.; Thoma, K. Deformation and melting of steel projectiles in hypervelocity cratering experiments. *Meteorit. Planet. Sci.* **2013**, *48*, 150–164. [[CrossRef](#)]
30. Axon, H.J.; Smith, P.L. A metallographic study of some iron meteorites of high nickel content. *Mineral. Mag.* **1972**, *38*, 736–755. [[CrossRef](#)]
31. Desrousseaux, A.; Doukhan, J.C.; Fieni, C.; Perron, C.; Jeannot, J.P.; Lavielle, B.; Renaud, D.; Van Duysen, J.C.; Caffee, M.; Nishiizumi, K. A New Iron Meteorite from France. *Meteorit. Planet. Sci.* **1996**, *31*, A36–A37.

